Vacancies and interstitial atoms in e^--irradiated germanium

P. Ehrhart, and H. Zillgen

Citation: Journal of Applied Physics **85**, 3503 (1999);
View online: https://doi.org/10.1063/1.369709
View Table of Contents: http://aip.scitation.org/toc/jap/85/7
Published by the American Institute of Physics

Vacancies and interstitial atoms in e^--irradiated germanium

P. Ehrhart[a] and H. Zillgen[b]
Institut für Festkorperforschung, Forschungszentrum Jülich GmbH, D 52425 Jülich, Germany

(Received 9 October 1998; accepted for publication 4 January 1999)

High purity Ge wafers have been irradiated at low temperatures with MeV electrons and have subsequently been investigated by x-ray diffraction methods. The intensity of the Huang diffuse scattering shows that a high concentration of defects ($>10^{19}$ cm^{-3}) can be frozen in at 4 K. A large fraction of the defects is stabilized in the form of close Frenkel pairs which are characterized by the nearly perfect cancellation of the long range displacement fields of the interstitial atom and the vacancy. We discuss the absolute size of these displacements as well as the introduction rate of the defects, which is of the order of $\Sigma=3$ cm^{-1}. The high defect introduction rates are at variance to the results of electrical and optical investigations and indicate that these methods detect only a few percent of the total defect concentration which is produced and frozen in at 4 K. The consequences for the understanding of the defect production in Ge and for the assumption of an athermal migration of interstitial atoms are discussed in close relation to similar results for Si. In addition, we discuss the differences between the defect patterns observed after 4 K irradiation to those observed after room-temperature irradiations and the thermally activated defect reactions up to the final annealing at 600 K. © *1999 American Institute of Physics.* [S0021-8979(99)04407-2]

I. INTRODUCTION

Point defects determine the electrical properties of semiconductors and the elemental semiconductors Si and Ge have therefore been investigated in great detail.[1] As the thermal equilibrium concentrations of the intrinsic point defects, vacancies and interstitial atoms are very low, most information has been obtained from low temperature electron irradiation experiments which produce pairs of vacancies and interstitial atoms, Frenkel pairs (FPs), in a reproducible manner. Ge was one of the first model substances for the investigation of irradiation effects in semiconductors[2,3] and some basic electrical properties have been determined in early experiments: independent of the initial doping Ge becomes highly ohmic and *p* type after high irradiation doses;[3] for *n*-type Ge, a defect introduction rate for 1 MeV electrons of $\Sigma=0.66$ cm^{-1} was deduced from electrical conductivity changes[4] which is quite close to later result of $\Sigma\approx1.0$ cm^{-1} from deep level transient spectroscopy (DLTS).[5] In addition, the formation and decay of vacancy-oxygen complexes at low temperatures was investigated by optical absorption spectroscopy.[6,7] With the increasing technological dominance of Si, the majority of investigations on defect properties changed to Si and this change was additionally motivated by the applicability of the electron paramagnetic resonance (EPR) to silicon.[1] Nevertheless, there are many defect properties controversially discussed even in Si and in spite of some differences these open questions are the same for Ge.

The published threshold energies for defect production vary between 13 and 30 eV,[3,5] however, the most reliable values for an effective threshold energy seem to be around 25 (Ref. 5) or 30 eV.[8] Hence, for typical electron energies of $E_e\approx1.5$ MeV, introduction rates $\Sigma\approx1$ cm^{-1} are expected. Such values are observed for *n*-type Ge, but for *p*-type and intrinsic Ge, the introduction rates are by at least two orders of magnitude lower. The low introduction rate has been explained—similar to Si—by a low temperature athermal, ionization-induced mobility of the interstitial atoms which yields a direct recombination of most of the Frenkel pairs.[5,9] This model is supported by indications for an enhancement of the defect mobility's by ionizing radiation at low temperatures.[10,11] Defects seem only to survive if the interstitial atom escapes direct recombination and arrives at another trap (e.g., a dopant atom) and forms a stable complex. Although there is at present no information on the structure or the properties of the isolated interstitial atom or the interstitial dopant complexes, there are indications for the interaction (kick-out or trapping) of interstitial atoms at low temperatures with group-III (Ga) as well as group-V (As, Sb) dopants.[12–14] Nevertheless, these are indirect conclusions and the explanation of the low apparent introduction rates by an insensitivity of the applied electrical methods in *p*-type or intrinsic Ge cannot be excluded.[8]

Considering this uncertainty about the defect scenario after low temperature irradiation, it is not astonishing that the defect mobility's and defect reactions during low temperature annealing are controversially discussed, too. Most information is available for *n*-type Ge and a first annealing stage at 65 K is attributed to the recombination of close Frenkel pairs due to interstitial mobility.[5,9] Vacancies are expected in the charge states V^{2-} or V^- in *n*-type Ge, and based on the optical detection of vacancy complexes, the mobility of these vacancies is attributed to annealing temperatures of 70 K[15] or between 100 and 120 K.[5,16] These reaction temperatures correspond to activation energies of 0.2–0.3 eV. The electrical

[a]Electronic mail: p.ehrhart@fz-juelich.de
[b]Present address: Siemens Matsushita Components, D-89508 Heidenheim, Germany.

data of Emtsev *et al.*[8] yield, however, a higher activation energy, V^-: 0.42 eV. There seems to be general agreement about the mobility of divacancies around 400 K. For intrinsic or *p*-type Ge, we expect the vacancy in the V^0 charge state and Emtsev *et al.*[8] suggest an activation energy for migration of 0.52 eV which is in agreement with recent perturbed γ–γ angular correlation (PAC) result which observe the trapping of vacancies at In atoms not below 200 K.[17] The annealing of the different DLTS spectra and their possible association with different defect charge states have been discussed in detail.[18]

As most of these spectroscopic studies are limited to low defect concentrations or irradiation doses ($\Phi t \leqslant 10^{17} e^-/\mathrm{cm}^2$), there is little known about the fate of FPs at higher doses, which is most relevant to the understanding of defect reactions after ion irradiations. Starting from the assumption about interstitial mobility during low temperature irradiation, there are two possibilities, i.e., the defect concentration saturates as there are no traps left (saturated traps), or larger clusters are formed around the impurities as nucleation centers (unsaturable traps). There is evidence for the formation of small defect agglomerates after very high dose irradiations in the high voltage electron microscope ($\Phi t \geqslant 10^{22} e^-/\mathrm{cm}^2$),[19] however, there are at present no quantitative results on the nucleation (intrinsic or extrinsic) and growth of these clusters. The present investigation is based on x-ray diffraction techniques, as these methods yield information on defect concentrations and defect structures and are applicable just within this gap of irradiation doses. In addition, first tests showed that the defect concentrations in Ge are large enough for an application of the method.[20]

In the following section we give a short introduction to the experimental methods and in Sec. III we present the experimental results. These new results are discussed in Sec. IV and are finally compared to similar investigations for Si[21–23] in order to elucidate some general trends.

II. EXPERIMENTAL METHODS

A. X-ray diffraction

If point defects are produced within a crystal, they induce first an overall expansion or contraction of the lattice which yields a change of the average lattice parameter and a corresponding shift of the Bragg peaks. Second, they induce local displacements of the atoms from the average lattice and as a consequence there is no longer perfect destructive interference between the Bragg peaks and there arises a diffuse scattering intensity. The investigations of the diffuse scattering intensity and of the change of the lattice parameter were performed with Cu $K_{\alpha 1}$ radiation at a measuring temperature of 8 K (for details, see, e.g., Refs. 24 and 25).

The theory necessary to exploit the information contained in the measured diffuse scattering cross section S is well documented,[26] and for small deviations, $\mathbf{q}$, of the scattering vector, $\mathbf{k}$, from a reciprocal lattice vector, $\mathbf{G}$, we observe the so-called Huang diffuse scattering (HDS). The scattering cross section of the HDS is given by $S_H(\mathbf{k}) = cf^2|\mathbf{ks(q)}|^2$; $\mathbf{s(q)}$ is the Fourier transform of the displacement field of an isolated defect, c is the defect concentration, and f is the atomic scattering factor. Due to the $1/r^2$ decrease of the long range displacement field around a point defect, we obtain the characteristic $1/q^2$ decrease of S_H.

$$S_H = cf^2(G/q)^2(1/\Omega^2)[\gamma^{(1)}\Pi^{(1)} + \gamma^{(2)}\Pi^{(2)} + \gamma^{(3)}\Pi^{(3)}]. \quad (1)$$

Ω is the atomic volume, $\gamma^{(i)}$ are factors which depend on the elastic constants and the directions of $\mathbf{q}$ and $\mathbf{G}$, and $\Pi^{(i)}$ are quadratic expressions of the components of the dipole force tensor, P_{ij}, which generally describes the elastic displacement field of a defect:

$$\Pi^{(1)} = \tfrac{1}{3}(Tr\mathbf{P})^2; \quad \Pi^{(2)} = \tfrac{1}{6}\sum_{i>j}(P_{ii} - P_{jj})^2;$$
$$\Pi^{(3)} = \tfrac{2}{3}\sum_{i>j}(P_{ij})^2. \quad (2)$$

By the measurements in different directions of $\mathbf{q}$ and/or $\mathbf{G}$, these parameters can be determined separately. The values of $\Pi^{(2)}$ and $\Pi^{(3)}$ determine the symmetry of the long range displacement field of the defect, e.g., both parameters are zero for cubic symmetry and both parameters are $\neq 0$ for orthorhombic symmetry.

For the following, the parameter $\Pi^{(1)}$ or the trace of the dipole force tensor is the most important parameter as it characterizes the strength of the displacement field and it is directly related to the relaxation volume of the defect:

$$V^{\mathrm{rel}} = TrP/(3B), \quad B = \text{bulk modulus}. \quad (3)$$

Neglecting the contribution of $\Pi^{(2)}$ and $\Pi^{(3)}$, we can write

$$S_H \sim c(V^{\mathrm{rel}})^2 G^2/q^2. \quad (4)$$

Hence, S_H yields the product $c(V^{\mathrm{rel}})^2$, and by combination with the change of the lattice parameter, $\Delta a/a \sim cV^{\mathrm{rel}}/3$, the two unknown numbers c and V^{rel} can be determined both. As we consider FPs, the experiment yields average values from the contributions of interstitial atoms and vacancies:

$$S_H \sim c[(V_i^{\mathrm{rel}})^2 + (V_v^{\mathrm{rel}})^2] \quad \text{and} \quad \Delta a/a \sim c(V_i^{\mathrm{rel}} + V_v^{\mathrm{rel}}). \quad (5)$$

These equations show that defects with opposite sign of V^{rel} can cancel in $\Delta a/a$, however, the diffuse scattering S_H adds up. Therefore S_H is a measure of the changes of the defect concentration even where $\Delta a/a$ vanishes.

This approach will be modified if the basic assumption of a random distribution of defects is no longer valid. Generally, c must be replaced in Eq. (1) by the Fourier transform of the concentration fluctuations which yield deviations from the characteristic $1/q^2$ behavior of S_H. We have to consider here two special situations:

(i) For the case of a clustering of defects, we observe a stronger increase of S_H at small values of q, and if and the total defect concentration is kept constant, a final enhancement:

$$S_H(\text{cluster}) = nS_H(\text{single defect}), \quad (6)$$

n is the number of defects in the cluster. Due to this enhancement HDS can very sensitively indicate the onset of cluster formation.

(ii) A close FP presents a special defect correlation as it combines defects with opposite signs of $\mathbf{s}$, which are sepa-

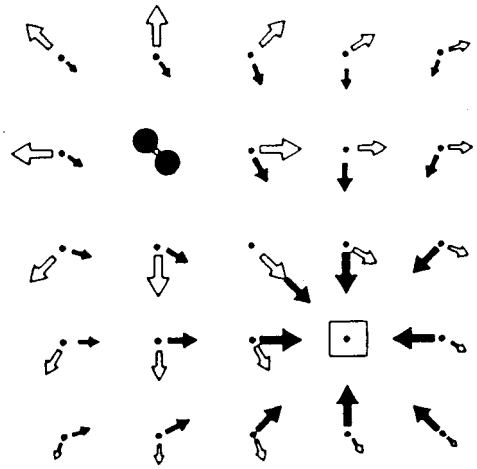

FIG. 1. Schematic view of the overlapping displacement fields of interstitial atoms and vacancies. The open arrows show the outward displacements of the interstitial atom, the filled arrows visualize the inward relaxations around the vacancy, and the magnitude indicates the size of the displacements. The displacements are additive between the defects and compensate at large distances.

rated by a certain minimum distance. Such a pair is characterized by large additive displacements between the vacancy and the interstitial atom and compensation of the displacements at larger distances (Fig. 1). These displacements yield a decrease of the intensity at small q values as discussed in detail for InP[24] and GaAs.[27]

B. Samples and irradiations

[001]-oriented samples were cut from Cz-grown high purity Ge crystals with a room-temperature resistivity of 50 Ω cm. They were n type with a carrier concentration of $n = 1.2\times10^{14}$ cm^{-3}. Sample sizes were $18\times5\times0.5$ mm^3. With the given nearly intrinsic conductivity only a small shift of the Fermi level can be expected after very low doses and we have highly ohmic Ge over the full range of doses investigated here. The irradiations were performed with 2.5 MeV electrons at the Jülich irradiation facility[28] with current densities between 5 and 10 μA/cm^2 (for details see Table I). After the low temperature irradiations, the samples were transferred to the measuring cryostat without intermediate warning. Measurements were performed at 8 K within a He gas atmosphere.

TABLE I. Samples and irradiations.

No.	Irrad. dose ($10^{19}e^-$/cm^2)	e^--energy (MeV)	Current density (μA/cm^2)	Irrad. temperature (K)
Ge-1	1.05	2.5	10	4
Ge-2	1.6	2.5	7	4
Ge-3	2.05	2.5	7	4
Ge-4	2.9	2.5	10	4
Ge-5	1.0	2.5	7	330

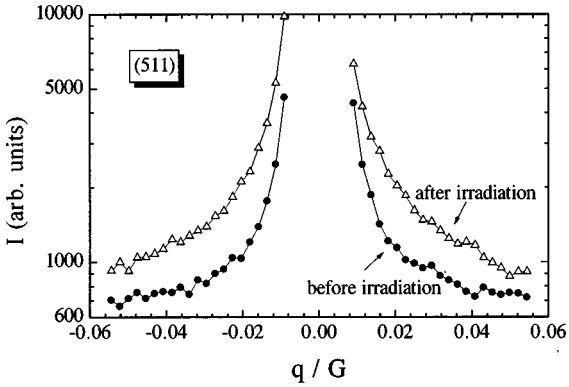

FIG. 2. Scattering intensity close to the (511) reflection of sample Ge-3 as measured at 8 K. The direction of the deviation vector **q** is parallel to the reciprocal lattice vector **G**. The background is identical before irradiation and after annealing at 600 K and the irradiation dose was $2.05\times10^{19}e^-$ cm^{-2}.

III. EXPERIMENTAL OBSERVATIONS

A. Defects after 4 K irradiation

Figure 2 shows an example of the irradiation-induced increase of the diffuse scattering close to the (511) reflection of sample Ge-3. The background is due to the thermal diffuse scattering and contains some tail of the Bragg peak which is several orders of magnitude higher in this plot. As these intensities have been shown to be generally independent of the irradiation within ≈1%, the defect induced scattering is directly obtained after the subtraction of this measured background. The scattering cross sections obtained after calibration are plotted in Fig. 3 for the (400) and (511) reflection. In order to compare the observed intensities directly to the expectation for a HDS behavior, the cross-section S is multiplied by q^2. In contrast to the expected straight line we observe a strong decrease of the intensity at small values of q and a pronounced asymmetry of the intensity for positive and negative deviations from the Bragg peak. From these features of the intensity (see Ref. 24 for a detailed discussion of the example of InP), we can conclude

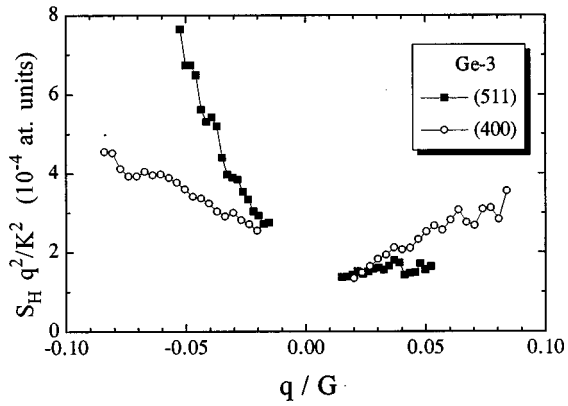

FIG. 3. Scattering function of the HDS, S_H, close to the (511) and (400) reflection of the irradiated sample Ge-3. The scattering function has been multiplied by q^2; for such a plot of S_Hq^2, a constant value is expected for isolated point defects.

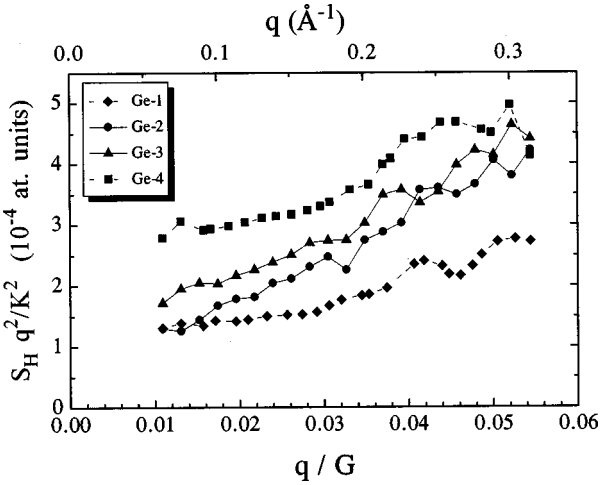

FIG. 4. Symmetrical part of the HDS observed close to the (511) reflections after different irradiation doses.

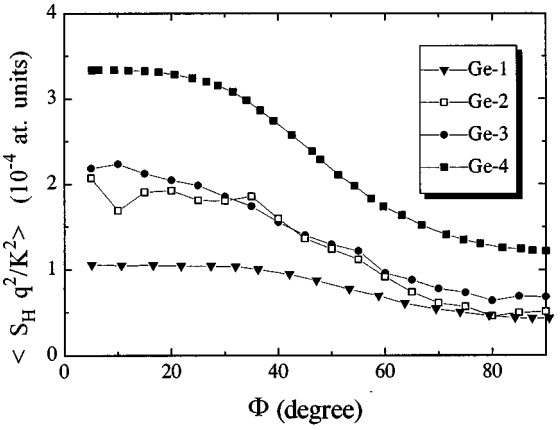

FIG. 6. Angular distribution of the symmetrical part of the scattering intensity around the (400) reflection of the irradiated sample Ge-3. Φ is the angle between the vector **q** and the reciprocal lattice vector **G** and similar to Fig. 5 average values are given for q values between 0.1 and 0.23 Å^{-1}.

that there is a dominant contribution of close FPs with a typical distance of 1–2 lattice constants present after irradiation. The characteristic compensation of the displacement fields due to interstitials and vacancies has been schematically shown in Fig. 1 and yields the decrease of the intensity at small q values; however, a determination of further details by a fit of defect models to the data seems not convincing due to the large number of free parameters for the description of such a displacement field. This situation may change as soon as there are detailed theoretical models for the atomic configurations available. Therefore, we concentrate on the symmetrical part of the intensity which is obtained by averaging at $+/-q$ and which is plotted for different irradiation doses in Fig. 4. Except for the points very close to the Bragg peak, we observe a linear increase of the intensity with irradiation dose which is shown for the data averaged over the given range of q values in Fig. 5. There is no indication of a faster increase at high doses as we would expect for defect clustering and as it is observed for Si. Figure 6 shows the angular distribution of the averaged intensities close to the (400) reflection. As this intensity is averaged at $+/-$ values of q and the intensities are symmetric relative to the [400] direction, this plot is shown as obtained after additional averaging over all four equivalent quadrants around the Bragg peak. There is no line of zero intensity as would be expected for cubic or tetragonal defects and the deduced low defect symmetry supports the model of the Frenkel pair whose long range symmetry is determined by the relative orientation of the pair. Combining all observations we conclude that we observe a nearly linear increase of S_H with irradiation dose up to $\Phi t = 3\times10^{19} e^-/\mathrm{cm}^2$, i.e., a continuous production of additional FPs.

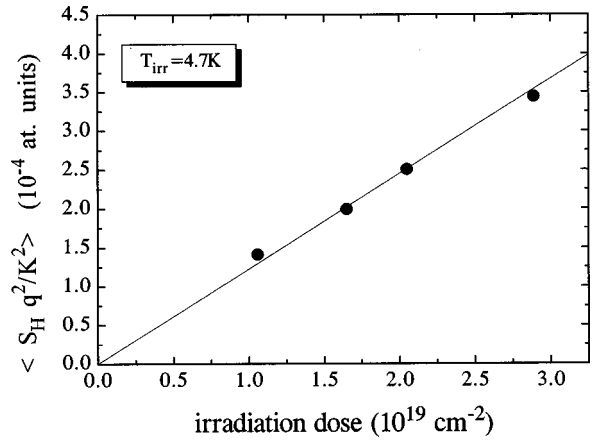

FIG. 5. Dose dependence of the HDS intensity for electron irradiated Ge. The points represent average values obtained from the intensities measured at (511) and (400) reflections and are averaged over q values ranging from 0.1 to 0.23 Å^{-1} (Fig. 4).

In contrast to the increase of S_H, we observe only a small change of the lattice parameter $[\Delta a/a \leqslant (0.9\pm0.5)\times10^{-5}]$ at a dose of $2\times10^{19} e^-/\mathrm{cm}^2$. These changes could not be investigated systematically as the other samples had larger errors probably due to some irradiation-induced strain. This small but positive change indicates that the outward displacements around the interstitial atoms are a little larger than the inward displacements around the vacancies. This is the opposite sign to Si where for the corresponding dose a change of $\Delta a/a = (-0.2\pm0.5)\times10^{-5}$ was observed. However, this small value shows that there is nearly cancellation in both cases as shown quantitatively below. The change of *(Δa/a)* can be compared to length changes, $\Delta l/l$, observed after irradiations with 4.5 MeV electrons up to a highest dose of $7.4\times10^{16} e^-/\mathrm{cm}^2$.[29] No change was observed for doped Ge but for intrinsic Ge a strong initial increase of the length was observed; however, there was indication for a saturation behavior already at these low doses at a value of $\Delta l/l \approx 1\times10^{-6}$ and the length measurements are therefore in good agreement with our observations.

B. Defect annealing

The defect reactions at higher temperatures were investigated within an isochronal annealing program within the He atmosphere of the cryostat. The holding times at the given temperatures, T_a, were 15 min and the measurements were repeated at 8 K. Figure 7 shows some examples of the

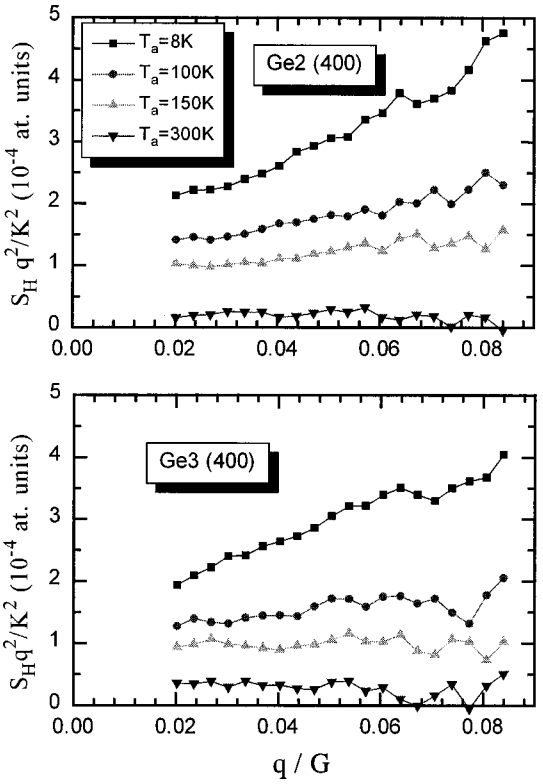

FIG. 7. Change of the distribution of the HDS (similar to Fig. 4) close to the (400) reflection of the samples Ge-2 and Ge-3 during annealing at the temperatures given in the inset.

change of the scattering function, S, during annealing. The most dramatic qualitative change is observed already below 100 K; the strong increase of the intensity at larger q values has nearly disappeared. This change indicates that the close pairs have essentially annealed and pairs with larger distances or weaker interaction survive. During annealing up to room temperature (RT), there is a further decrease of the intensity but there is no indication for an increase of the intensity at small q values which would directly indicate a growth of larger agglomerates. Hence the dominating defect reaction is further recombination of FPs and there are only about 10% of the defects left at RT.

Figure 8 summarizes the annealing behavior of the average values of the diffuse scattering intensity. There is annealing already at the first step to 15 K and a first well-established annealing stage is finished around 50 K, and this low temperature stage amounts to about 50% of the defects. The differences between the different samples show no systematic dependence on the irradiation dose and the remaining small differences might be attributed to temperature instabilities during the long irradiation times. There are only small changes between 50 and 100 K where a second stage starts which extends up to 300 K. The remaining damage anneals continuously in the range up to 600 K.

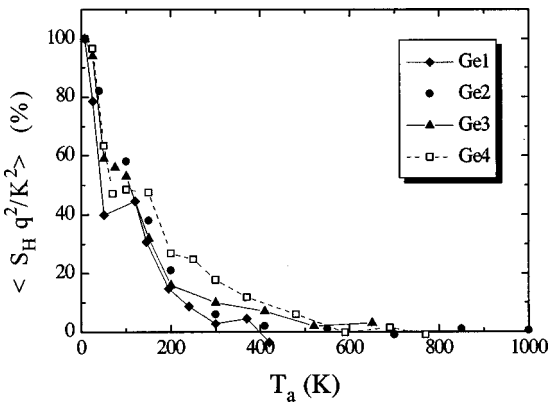

FIG. 8. Annealing of the average value of the HDS as defined in Fig. 5. Data are normalized by their value after irradiation.

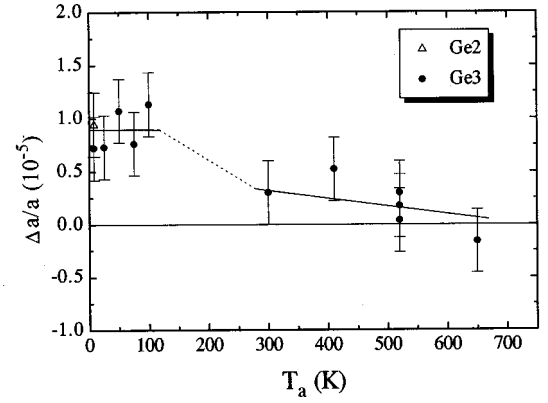

FIG. 9. Annealing of the average value of the change of the lattice parameter measured for samples Ge-2 and Ge-3.

The annealing of the change of the lattice parameter is summarized in Fig. 9. In spite of the large error bars, there is an indication of a difference to the HDS: there is no change within the low temperature stage up to 100 K and essential annealing only between 100 and 300 K. This means that there are differences between the close pairs annealing at low temperatures and the more separated FPs, i.e., there is complete compensation for the close pairs and a small positive difference for the more separated defects.

Although there is within the errors complete annealing at 600 K for the HDS as well as for the lattice parameter, the electrical resistivity has not yet annealed: as expected, the conductivity had converted to p type during irradiation and stayed p type after annealing at 440 K ($\rho=1.2\ \Omega\,\mathrm{cm}$, $p \approx 2.9\times10^{15}\ \mathrm{cm}^{-3}$) and even at 770 K ($\rho=45.4\ \Omega\,\mathrm{cm}$). This behavior is in good agreement with the observations after neutron transmutation doping.[30] Hence the initially present impurities had been transformed by reactions with mobile irradiation defects, however, the resulting low concentration of defect complexes cannot be detected by the XRD methods.

C. Defects after RT irradiation

As expected from the strong annealing below RT, the defect production at 330 K is much lower than at 4 K, nevertheless, there is an increase of the HDS as shown in Fig. 10. Again, the distribution is described by a simple q^{-2} behavior. In addition, the intensity is very similar to that obtained after 4 K irradiation and subsequent annealing to 330 K. The observed change of the lattice parameter $\Delta a/a=(2\pm3)\times10^{-6}$ is also not different from the value observed

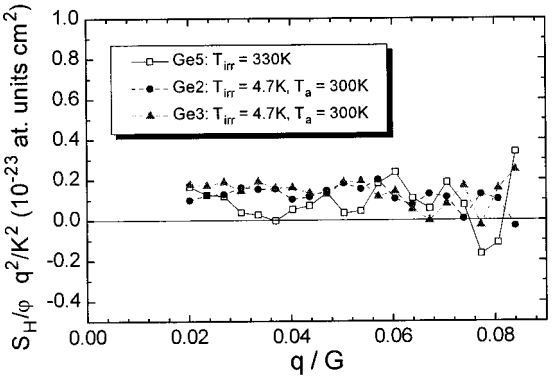

FIG. 10. Scattering function of the HDS (similar to Fig. 4) as observed close to the (400) reflection of the RT irradiated sample Ge-5. Data obtained after 4 K irradiation and subsequent annealing at RT are shown for comparison.

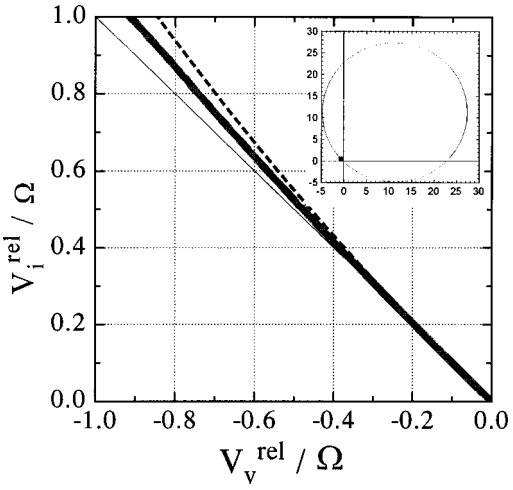

FIG. 11. Values of the relaxation volumes, V_i^{rel} and V_v^{rel}, which are compatible with the measured values of S_H and $\Delta a/a$; the inset shows all possible solutions and the figure shows the range of the reasonable solutions in an enlarged scale. The thick line corresponds to the average over all defects. In addition, there is a thin straight line which corresponds to complete compensations of the displacement fields of the interstitial and the vacancy as it is observed for the close FPs which anneal below 100 K, and a dashed line which represents the defects annealing above 100 K.

after irradiation and annealing to RT (Fig. 9). Hence, we simply can assume that it is essentially the same kind of defect which survives independent of the irradiation and annealing conditions, and there is no indication of a nucleation and growth of larger agglomerates due to the higher defect mobility during RT irradiation.

IV. DISCUSSION OF THE EXPERIMENTAL RESULTS

A. Quantitative results for the introduction rates and defect strengths

1. Average over all defects at present 8 K

The quantitative data for the defect strength and the symmetry parameters are summarized in Table II. The errors have been estimated from the differences between the results obtained from measurements at different reflections. In order to get a measure for the defect concentration which is independent of the actual irradiation dose, we use in the following discussion the introduction rate $\Sigma = c/\Phi t$. Combining these results from HDS and lattice parameter according to Eq. (5), we can display all nonimaginary solutions of this quadratic equation system on a circle as shown in the inset of Fig. 11. We exclude all solutions corresponding to a positive V_v^{rel} and a negative V_i^{rel} as no theoretical expectation supports such a choice. Although the positive value of Δa indicates larger values for the interstitial relaxation than for V_v^{rel}, these vacancy relaxations cannot be negligible. Assuming $V_v^{\mathrm{rel}} = 0$, Fig. 11 yields an interstitial relaxation of 22 Ω which is characteristic for clusters containing the given number of interstitial atoms and is not compatible with a point defect like scattering pattern as discussed in Sec. III. In order to further restrict the range of reasonable solutions, we have to consider the corresponding defect concentrations and there is an obvious upper limit for the introduction rate if we calculate the production cross section for a given threshold energy.[31] Hence, starting from the possible solutions shown in the inset we end up with the range of reasonable solutions shown in the main part of Fig. 11. In this range of values, we observe only a small difference between the straight line corresponding to the exact compensation of interstitials and vacancies and the exact calculation which yields a difference of about 5% at most. Figure 12 shows the corresponding introduction rates as a function of the assumed relaxation volume of the interstitial atom. An arrow indicates the introduction rate which corresponds to the lower limit of the values discussed for the threshold energy (≈25 eV) and which therefore may be considered as an upper limit for Σ. On the other hand, the inward relaxation around the vacancies is limited, too. $|V_v^{\mathrm{rel}}| = |-0.5\ \Omega|$ seems to be an upper limit for the absolute value of the relaxation's considering the experimental results which have been obtained mostly for metals and which is consistent also with the discussion of the electronic properties of vacancies in Si (Ref. 1) (however, there are recent calculations for Si[32] which yield a value of $-0.95\ \Omega$, which means that there would be no density difference left at the vacancy). Considering these arguments there remains a limited range for the reasonable values of the relaxation volumes and introduction rates which is indicated by the broadened line in Fig. 12, i.e., the final values must be situated around:

$$V_i^{\mathrm{rel}} = -V_v^{\mathrm{rel}} = 0.5\ \Omega \quad \text{and} \quad \Sigma = 3\ \mathrm{cm}^{-1}.$$

The linear dose dependence of the HDS for doses up to $3 \times 10^{19} e^-/\mathrm{cm}^2$ (Fig. 5) demonstrates that, in contrast to the expectation, we observe neither a saturation of the defect

TABLE II. Results from HDS and $\Delta a/a$.

No.	Φt ($10^{19} e^-/\mathrm{cm}^2$)	$2\Sigma\ (V^{\mathrm{rel}}/\Omega)^2$ (cm^{-1})	Π^2/Π^1	Π^3/Π^1	$(\Delta a/a)/\Phi t$ (10^{-24} cm^2)
Ge-1	1.05	1.57±0.30	0.75±0.35	0.12±0.10	0.10±0.3
Ge-2	1.6	1.40±0.12	0.12±0.40	0.09±0.30	0.50±0.2
Ge-3	2.05	1.30±0.18	0.11±0.50	0.08±0.15	0.45±0.2
Ge-4	2.9	1.55±0.12	0.45±0.15	0.10±0.10	0.70±0.4
Ge-5	1.0 at RT	0.12±0.03	⋯	⋯	0.20±0.2
Ge-2,3	Anneal: RT	0.14±0.04	⋯	⋯	0.15±0.2

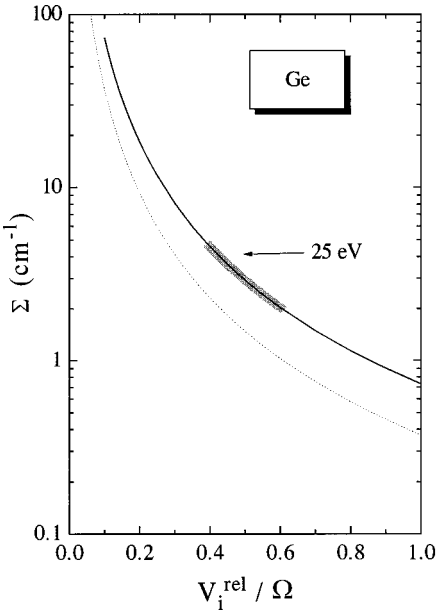

FIG. 12. Dependence of the introduction rate Σ on the assumption on the relaxation volume of the interstitial atom ($V_i^{rel} \approx -V_v^{rel}$ can be assumed for simplicity). The arrow indicates the value for the introduction rate which corresponds to a threshold energy for atomic displacements of 25 eV and the thick bar indicates the region of the most probable values. The dotted line corresponds to the close FPs which anneal below 100 K.

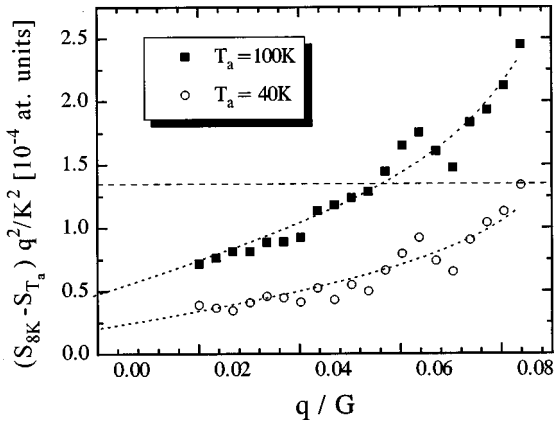

FIG. 13. Distribution of the scattering intensity close to the (400) reflection of sample Ge-2. These curves have been obtained by subtracting the intensity left at the given annealing temperature from the intensity observed initially at 8 K. The average value for the intensity observed after annealing at 100 K is indicated by the dashed line. The dotted lines indicate the extrapolated intensities at $q=0$.

concentration at the concentration of the doping atoms ($\leqslant 10^{15}$ cm^{-3}), nor the beginning of cluster growth at the corresponding dose. The observation of more than 10^{19} FPs/cm^3 clearly shows that these defects are intrinsic and not stabilized by impurities.

2. Close Frenkel pairs

We observe essentially two annealing stages: one between 8 and 55 K and a second one between 100 and 300 K. However, the first one is not observed in Δa, and we conclude that the defects which recombine within this stage have perfect interstitial-vacancy compensation, $V_i^{rel} = -V_v^{rel}$ (corresponding to the straight line in Fig. 11), and we consider them as close FPs. These close FPs present about 50% of the defects produced and the corresponding introduction rates are included in Fig. 12 as a dotted line.

Assuming that we have only close pair recombination and no rearrangement of the surviving defects between 8 and 100 K, we can deduce a more detailed scattering function of the vanishing defects from the difference between S(8 K) and S(100 K), which is shown in Fig. 13. Similar differences have also been taken at some additional lower temperatures and the difference at 40 K is included in Fig. 13. The similarity of the slopes of all differences supports the assumption that there is always the same type of defect annealing. The extrapolation of the experimental points to $q=0$ is shown by a dotted line in Fig. 13. This nonvanishing extrapolated intensity indicates that not all defects are closely correlated pairs. These defects must be somewhat further separated in order not to show the totally destructive interference within the region of the measurements. The comparison of this extrapolated intensity to the average value which is indicated as a dashed line in Fig. 13 yields that about 70% of the FPs are closely correlated within 1–2 lattice constants. Due to the larger uncertainties of the measurements of the lattice parameter, a part of the effect might also be due to a deviation from the assumed perfect compensation.

3. Defects which anneal between 100 K and RT

Within this region about 50% of the total HDS and the total change of the lattice parameter are observed to anneal. Therefore, the correction for the incomplete compensation is larger (the results for V^{rel} are shown in Fig. 11 as a dashed line) and corresponds to a change in V_i^{rel} of about 10%. Using the same arguments as above we end up with a similar optimum choice of values:

$$V_i^{rel} = 0.55\ \Omega, \quad V_v^{rel} = -0.50\ \Omega, \quad \text{and} \quad \Sigma = 1.3\ \text{cm}^{-1}.$$

These values indicate no dramatic changes during annealing and thus supports the assumptions made above.

B. Thermally activated defect reactions

We first discuss the low temperature stage between 8 and 100 K which has been shown to correspond essentially to the recombination of close pairs. The characteristic scattering function of these close FPs has been discussed above (Figs. 7 and 13) and the different scattering function observed at higher temperatures are shown in Fig. 7. From our observation of the recombination of defects we cannot directly deduce which is the mobile defect, but considering the evidence for interstitial mobility in the literature[16,13] we attribute this recombination to the mobility of the interstitial atom. Remarkable is, however, that there is about 50% annealing below 55 K whereas the main stage observed by electrical measurements is observed around 65 K and only small additional stages have occasionally been observed around 14, 27, and 35 K.[16,13] This observation supports the conclusion from the large difference in the introduction rates that the electrical measurements cannot detect the majority defect, especially the intrinsic FPs.

Within the second stage (100–300 K), which is broader and certainly cannot be attributed to a single defect reaction, additional 40% of the HDS anneal and the lattice parameter anneals in parallel. Within this temperature range vacancy migration is expected.[5,8,16–18] The defects remaining above 150 K show no longer an indication of vacancy-interstitial correlation and therefore annealing should occur via long range migration. Nevertheless, we have no indication of the formation of larger agglomerates of like defects although a detailed analysis of the 10% of the scattering intensity remaining at RT implies larger uncertainties. The total number of defects remaining at RT of $\approx 10^{18}$ cm^{-3} is still orders of magnitude above the impurity level and only immobile intrinsic complexes should therefore be considered. From the intensity distributions of Fig. 7 which indicate some weak defect correlation up to 150 K, we might attribute the annealing up to 200 K to interstitial mobility and especially the range 150–200 K to a free migration. The final annealing between 200 and 300 K is then attributed to vacancy migration in agreement with the data for the vacancy migration energy for *p*-Si (0.42–0.52 eV)[8] and the results of PAC investigations[17] which indicate the formation of In-vacancy complexes above 200 K. The attribution of free interstitial migration to the temperature range between 100 and 200 K is not in contradiction to the latest explanation of the higher frequency PAC signal which appears around 220 K by a self-interstitial In complex[17] as we have to consider the longer diffusion lengths to the distributed In atoms and possibly a complicated trapping kinetics. Within this scenario we expect only small complexes surviving at RT, i.e., essentially diinterstitial atoms and divacancies. Consequently, nearly complete annealing can be observed along with the migration of the divacancy around 400 K.[3,5,16] Finally, there is a remarkable similarity between the scattering observed after annealing at RT and the RT irradiation Fig. 10. This observation seems in contrast to the simple expectation that during irradiation at elevated temperatures a thermally activated defect mobility in addition to the possible athermal interstitial mobility should reduce the stationary defect concentration and consequently the nucleation probability of clusters. The fraction of 10% of the damage observed at 8 K might, however, indicate that these small agglomerates might be directly nucleated due to double displacements as we expect this order of magnitude of multiple displacement events[31] for our electron energies of 2.5 MeV and assuming a threshold energy of 25–30 eV.

V. CONCLUSIONS

We have shown that a high concentration of intrinsic bound FPs which had not been observed earlier can be produced in Ge. In spite of their ''electrical invisibility,'' these FPs may have important consequences for the modeling of defect reactions during irradiation or ion implantation and annealing. The most important result for the defect structure and concentration, the possible athermal ionization-induced mobility, and the thermally activated reaction may be summarized.

(i) The diffuse scattering shows that the displacement fields of interstitial atoms and vacancies in Ge cancel nearly exactly and we have discussed that the absolute size of the related relaxation volumes: $V_i^{\mathrm{rel}} = -V_v^{\mathrm{rel}} = 0.5\ \Omega$. At low temperature, a large part of these defects is in the form of close FPs and the total introduction rate is for 2.5 MeV electrons in the order of $\Sigma = 3$ cm^{-1}. This value corresponds to an effective threshold energy for the defect production of $\approx$30 eV. Except for the small differences in the amount of deviation from the perfect compensation of interstitials and vacancies, this behavior is the same as for Si.[21,22] Although we have investigated here only intrinsic Ge, we can assume that similar to Si this behavior is unchanged for highly doped crystals.

(ii) The introduction rate of these defects shows no indication of saturation up to electron doses of 3×10^{19}/cm^2 and we can freeze in defect concentrations of 9×10^{19}/cm^3. This high introduction rate for intrinsic or slightly *p*-type Ge indicates that many electrical methods observe only a small percentage of the defects introduced at low temperatures and we have to ask: why have these high defect concentrations not been observed by other methods. From the observed compensation of the displacements of interstitials and vacancies, it is obvious that the very precise early lattice parameter measurements[29] could only observe small effects and saturation at defect concentrations similar to the doping level. As electrical and spectroscopic methods rely on charged defects and/or energy levels within the band gap, we might speculate about the FP as an acceptor-donor pair which appears nearly neutral from the outside and consequently these FPs are not detected. Remarkably, such acceptor-donor pair properties as well as the compensation of the displacement fields have recently also been found in tight-binding molecular dynamics simulations for Frenkel defects in Si.[32]

(iii) Our results can be most straightforwardly explained by the continuous production of stable FPs and therefore one of the arguments for a high athermal mobility of the interstitial atom which explains a spontaneous recombination is no longer valid for Ge. Nevertheless, we cannot exclude this process which can explain a large reaction rate of interstitial atoms with dopant atoms during irradiation. Similar to the situation with Si we may have detrapping from vacancies and retrapping of interstitials at vacancies which become the dominant trap type at high doses.[21,22] Hence, we finally will end up again with dominating close pairs in spite of a high trapping probability at dopants. As similar arguments must be applied also for III–IV compounds[24,27] this athermal detrapping-retrapping reaction might be a quite general behavior in irradiated semiconductors.

(iv) At the highest doses, we observe some difference to Si where an increase of the intensity is observed which is a result of the formation of defect clusters.[22] This difference indicates a smaller escape probability of interstitial atoms in Ge at low temperatures and/or a higher nucleation barrier for the formation of small interstitial complexes. However, similar clustering effects might be observed with a factor of 2 increase in the dose and transmission electron microscope (TEM) results indicate that there are only small quantitative differences. In contrast to Si no clusters were observed in Ge

after similar irradiations in the high voltage TEM,[33] whereas at somewhat higher doses clusters could be produced also in Ge.[19]

(v) Thermally activated defect reactions up to RT are dominated by the recombination of FPs. This observation allows, however, no direct conclusion on the mobile defect. Nevertheless, considering all available data a simple reaction scheme evolves. Close FPs anneal between 10 and 55 K indicating a spectrum of recombination barriers between 0.06 and 1.5 eV. Less closely related pairs anneal slowly up to 150 K and longer range interstitial migration dominates up to 200 K where the vacancy migration starts. This scheme shows much similarity to lower dose irradiations of Si. For low dose irradiated Si, we observe a similar close pair annealing below 50 K, however, the amount of annealing is strongly dose dependent.[22] Long range interstitial migration seems to start around 100 K and for intrinsic samples there is a first indication for interstitial clusters at 100 K. The vacancy migration in Si is still open for discussion: EPR data suggest migration between 100 K and RT dependent on the doping, however, the very strongly suppressed annealing for the high irradiation dose might indicate that vacancies migrate only above RT.

(vi) For the low dose irradiations, complete annealing is observed within the errors of the XRD experiments at similar temperatures for Ge and Si and can be attributed to the migration of dimers. However, the complexes observed at higher doses in Si show a much higher stability. In summarizing, the thermally activated reactions support the conclusions from the irradiation behavior, which showed a tendency for a lower escape probability of the interstitial from FPs and a more difficult nucleation of interstitial complexes. This behavior is also reflected in the defect pattern observed after RT irradiations of Ge which simply can be attributed to the defects directly produced in double displacements. This behavior is in contrast to Si where defect dopant complexes are important.

ACKNOWLEDGMENTS

The authors thank Professor W. Schilling for many helpful discussions and they gratefully acknowledge the technical assistance by W. Bergs and U. Dedek and last but not least, they greatly appreciate the continuous support by Dr. F. Dworschak and B. Schmitz in the course of the electron irradiations.

[1] G. D. Watkins, in *Electronic Structure and Properties of Semiconductors*, edited by W. Schroeter, Vol. 4 of Materials Science and Technology (VCH, Weinheim, 1992), p. 105.
[2] W. E. Johnson and K. Lark Horowitz, Phys. Rev. **83**, 312 (1951).
[3] J. W. Corbett, *Electron Radiation Damage in Semiconductors and Metals*, Vol. 7 of Solid State Physics, Advances in Research and Applications (Academic, New York, 1966).
[4] T. A. Calcott and J. W. MacKay, Phys. Rev. **161**, 698 (1967).
[5] J. C. Bourgoin, P. M. Mooney, and F. Poulin, Inst. Phys. Conf. Ser. **59**, 33 (1981).
[6] R. E. Whan, Phys. Rev. **140**, A690 (1965).
[7] R. E. Whan, in *Electron Radiation Damage in Semiconductors*, edited by F. L. Vook (Plenum, New York, 1968), p. 195.
[8] V. V. Emtsev, T. V. Mashovets, and V. V. Miknovich, Sov. Phys. Semicond. **26**, 12 (1992).
[9] P. M. Mooney, F. Poulin, and J. C. Bourgoin, Phys. Rev. B **28**, 3372 (1983).
[10] W. D. Hyatt and J. S. Koehler, Phys. Rev. B **4**, 1903 (1971).
[11] J. M. Meese, Phys. Rev. B **9**, 4373 (1974).
[12] A. Hiraki, J. W. Cleland, and J. H. Crawford, in *Electron Radiation Damage in Semiconductors*, edited by F. L. Vook (Plenum, New York, 1968), p. 224.
[13] N. Fukuoka and H. Saito, Inst. Phys. Conf. Ser. **31**, 285 (1977).
[14] N. Fukuoka, H. Saito, and T. Tsuchida, Radiat. Eff. **36**, 23 (1978).
[15] J. W. Corbett, J. P. Karins, and T. Y. Tan, Nucl. Instrum. Methods **182/183**, 457 (1981).
[16] J. W. Corbett and J. C. Bourgoin, in *Point Defects in Solids*, edited by J. H. Crawford and L. M. Slifkin (Plenum, New York, 1975), Vol. 2, p. 1.
[17] H. Häßlein, R. Sielemann, and Ch. Zistl, Mater. Sci. Forum **258/263**, 59 (1997).
[18] N. Fourches, G. Walter, and J. C. Bourgoin, J. Appl. Phys. **69**, 2033 (1991).
[19] M. Hirata and M. Kiritani, Physica B **116**, 616 (1983).
[20] S. Bausch, H. Zillgen, and P. Ehrhart, Mater. Sci. Forum **196/201**, 114 (1995).
[21] H. Zillgen and P. Ehrhart, Nucl. Instrum. Methods Phys. Res. B **127/128**, 27 (1997).
[22] P. Ehrhart and H. Zillgen, Mater. Res. Soc. Symp. Proc. **469**, 175 (1997).
[23] H. Zillgen and P. Ehrhart, Mater. Sci. Forum **258/263**, 503 (1997).
[24] K. Karsten and P. Ehrhart, Phys. Rev. B **51**, 10508 (1995).
[25] P. Ehrhart, J. Nucl. Mater. **216**, 170 (1994).
[26] P. H. Dederichs, J. Phys. F **3**, 471 (1973).
[27] A. Pillukat, K. Karsten, and P. Ehrhart, Phys. Rev. B **53**, 7823 (1996).
[28] J. Hemmerich, W. Sassin, and W. Schilling, Z. Angew. Phys. **29**, 20 (1970).
[29] J. C. North and R. C. Buschert, J. Appl. Phys. **37**, 639 (1966).
[30] H. Saito, N. Fukuoka, and H. Yoshida, Inst. Phys. Conf. Ser. **59**, 45 (1981).
[31] O. S. Oen, Report: ORNL-4897, 1973.
[32] M. Tang, L. Colombo, J. Zhu, and T. Diaz de la Rubia, Phys. Rev. B **55**, 14279 (1997).
[33] H. Föll, Inst. Phys. Conf. Ser. **23**, 233 (1975).